

Pairing Symmetry in Single-Layer Tetragonal $\text{Ti}_2\text{Ba}_2\text{CuO}_{6+\delta}$ Superconductors

C. C. Tsuei,* J. R. Kirtley, M. Rupp, J. Z. Sun, A. Gupta, M. B. Ketchen, C. A. Wang, Z. F. Ren, J. H. Wang, M. Bhushan

A high-resolution scanning superconducting quantum interference device microscopy study of tetragonal single-layer $\text{Ti}_2\text{Ba}_2\text{CuO}_{6+\delta}$ films, deposited on tricrystal SrTiO_3 substrates, demonstrates the effect of spontaneously generated half flux quanta. This observation shows that in addition to $\text{YBa}_2\text{Cu}_3\text{O}_7$, the order parameter symmetry in $\text{Ti}_2\text{Ba}_2\text{CuO}_{6+\delta}$ is consistent with that of a $d_{x^2-y^2}$ pair state. This result also rules out any bilayer or twinning effects and any pairing that is incompatible with the fourfold rotational symmetry as in the $\text{Ti}_2\text{Ba}_2\text{CuO}_{6+\delta}$ superconducting system.

An unambiguous determination of the pairing symmetry in copper oxide superconductors is necessary to understand the origin of high-temperature superconductivity. A test of order parameter symmetry requires a definitive measurement of the phase of the energy gap in the superconducting state. Recently, several phase-sensitive experiments (1–7) have produced strong evidence for d -wave pairing symmetry. Wollman *et al.* (1) reported a phase-sensitive measurement using the interference effect in $\text{Pb-YBa}_2\text{Cu}_3\text{O}_{7-\delta}$ superconducting quantum interference devices (SQUIDs), suggesting a d -wave order parameter symmetry. This was followed by several more convincing pairing symmetry experiments using tricrystal ring magnetometry (2, 3), SQUID interferometry (4, 5), and single junction modulation (6, 7). However, all these experiments were limited to the $\text{YBa}_2\text{Cu}_3\text{O}_{7-\delta}$ (YBCO) system. The crystal structure of YBCO is orthorhombic (the a and b directions in the CuO_2 planes are structurally and electronically inequivalent because of the presence of CuO chains) and there are two CuO_2 planes per unit cell. According to several recent theoretical models (8–10), these two features of the YBCO crystal structure can complicate, even invalidate, the conclusion of d -wave pairing symmetry determined from the phase-sensitive experiments. Strictly speaking, the twofold rotational symmetry of an orthorhombic crystal supports an admixture of s - and d -wave pair states but

C. C. Tsuei, J. R. Kirtley, M. Rupp, J. Z. Sun, A. Gupta, and M. B. Ketchen are at IBM Research Division, Thomas J. Watson Research Center, Yorktown Heights, NY 10598, USA. C. A. Wang, Z. F. Ren, and J. H. Wang are at Superconducting Materials Laboratory, Natural Sciences and Mathematics Complex, State University of New York, Buffalo, NY 14260, USA. M. Bhushan is at Department of Physics, State University of New York, Stony Brook, NY 11794, USA.

*To whom correspondence should be addressed.

not a pure two-dimensional d -wave pairing symmetry ($d_{x^2-y^2}$), which has a fourfold rotation axis. In addition, as a result of certain bilayer and chain effects, it is possible, for example, to have two sets of order parameters with opposite signs that can mimic the observed $d_{x^2-y^2}$ gap structure (8, 9). This situation can be resolved by a d -wave tricrystal experiment with a tetragonal single-layer cuprate system such as $\text{Ti}_2\text{Ba}_2\text{CuO}_{6+\delta}$ (Ti2201). Here, we present results of such a tricrystal experiment to show that, as in the case of YBCO, the half-integer flux quantum effect has been observed in the Ti2201 system and its pair wave function has nodes and lobes consistent with a d -wave pairing symmetry.

Theory behind the test of pair wave function symmetry. The details of our tricrystal experiments have been described elsewhere (2, 3, 11). In essence, these experiments were designed to decipher the microscopic phase information of a pair wave function by combining two macroscopic quantum coherence measurements (that is, flux quantization and pair tunneling) in a superconducting cuprate ring interrupted by three grain boundary junctions. On the basis of the considerations of free energy (12) and flux quantization (2), it has been shown that the ground state of a superconducting ring with an odd number of π -junctions is doubly degenerate and should exhibit a spontaneous magnetization of one-half flux quantum, $\pm(\Phi_0/2 = h/4e)$ (where h is Planck's constant and e is the fundamental charge of an electron or proton), provided that $L(I_c)_{\min} \gg \Phi_0$, where L is the self-inductance of the ring and $(I_c)_{\min}$ is the critical current of the weakest junction in the ring. A π -junction is a Josephson junction with a negative pair tunneling current. The Josephson current, I_s , of a junction made of two superconductors i

and j can be expressed as

$$I_s^{ij} = |I_c^{ij}(\theta_i, \theta_j)| \sin(\Delta\phi_{ij} + \phi_j) \quad (1)$$

where θ_i and θ_j are the angles of the crystallographic axes with respect to the junction interface, $\Delta\phi_{ij}$ is phase difference at the junction, and the gauge-invariant phase is

$$\phi_j = \begin{cases} 0 & \text{if } I_c^{ij} > 0 \\ \pi & \text{if } I_c^{ij} < 0 \end{cases} \quad (2)$$

As is obvious from Eq. 1, the negative sign of I_c^{ij} can be considered a phase shift of π added to $\Delta\phi_{ij}$ —hence, the terminology π -junction.

The supercurrent of a junction made from s -wave superconductors with an isotropic or anisotropic gap is always positive, and such junction is called a zero-junction. In 1987, Geshkenbein, Larkin, and Barone (13) suggested that it is possible to have a negative supercurrent for a Josephson junction made of a non- s -wave superconductor (that is, a superconductor with nodes in the gap function). More recently, Sigrist and Rice (12) have shown specifically that for the case of a junction between two d -wave superconductors i and j , the maximum Josephson current $I_c^{ij}(\theta_i, \theta_j)$ can be expressed as

$$I_c^{ij}(\theta_i, \theta_j) \propto \cos 2\theta_i \cos 2\theta_j \quad (3)$$

In the maximum disorder limit for a tetragonal crystal, Eq. 3, the Sigrist-Rice clean limit formula is replaced by

$$I_c^{ij}(\theta_i, \theta_j) \propto \cos 2(\theta_i + \theta_j) \quad (4)$$

Based on Eqs. 3 and 4, a tricrystal (100) SrTiO_3 substrate was designed to test the d -wave pairing symmetry in YBCO. The misorientation angles and the angle between the grain boundary planes were chosen so that a YBCO tri-junction ring located at the tricrystal meeting point contained one or three π -junctions (Fig. 1). In addition, three rings with even-number junctions (two rings located at the bicrystal grain boundaries and one in the grain) were fabricated as a control. A scanning SQUID microscope (SSM) (14) was used to non-invasively measure the ground state of the rings at 4.2 K and near zero magnetic field. The fact that only spontaneous magnetization of a one-half magnetic flux quantum ($\Phi_0/2$) has been directly observed in the three-junction ring, but not in the control rings, supports d -wave pairing in YBCO.

Tricrystal experiment using Ti2201. Here we present our results on the tricrystal experiment with Ti2201 instead of YBCO. The Ti2201 single-layer, tetragonal, epitaxial films used in this experiment were prepared with radiofrequency magnetron sputtering and a two-step post-annealing in a low-pressure Ar atmosphere to promote epitaxial film growth and to adjust the stoichiometry. By careful control of the oxygen content (δ) in the post-annealed films, the

superconducting transition temperature can be varied from ~ 0 to 80 K reproducibly. Some results of the x-ray diffraction (XRD) measurements on the Tl2201 films indicate that the intensity as a function of 2θ shows only (001) reflection peaks (Fig. 2). A rocking curve (x-ray ω scan) of the (0010) reflection of a Tl2201 film grown on a single-crystal SrTiO₃ substrate has a full width at half-maximum equal to 0.265°.

All these XRD data suggest that the Tl2201 films are characterized by high-quality, *c*-axis-oriented epitaxial film growth. The four sharp ϕ -scan peaks 90° apart from the reflection of (105) of the Tl2201 epitaxial films suggest strong in-plane alignment of the Tl2201 film with the substrate. To rigorously prove that our epitaxial film is tetragonal using only the XRD data is impossible because the splitting of certain XRD reflections due to orthorhombicity is not observable in our epitaxial films. For example, when the tetragonal to orthorhombic phase transition takes place, the (110) reflection is replaced by (020) and (200) peaks, which are not allowed in *c*-axis-oriented epitaxial films. We also unsuccessfully attempted to detect the orthorhombic structure with the x-ray ϕ -scan measurement. It turned out that the estimated difference in ϕ values between the two structures is about the same as the observed peak width in the ϕ scan. However, the tetragonality of our Tl2201 epitaxial films was finally ensured with the use of Raman spectroscopy, by establishing a one-to-one correspondence in the values of critical temperature (T_c), and the positions of the Raman peaks (associated with the O2 and O3 phonon modes in the Ba-O and Tl-O planes, respectively) between our films and the tetragonal polycrystalline bulk samples that were prepared under similar annealing conditions for making the films (15).

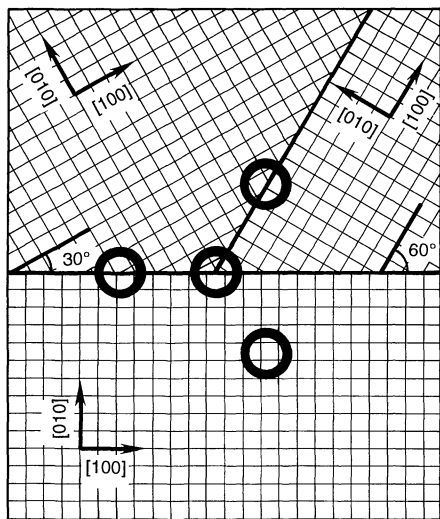


Fig. 1. A schematic sketch of the tricrystal (100) SrTiO₃ substrate, showing the locations of the zero-, two-, and three-junction rings.

After the Tl2201 film was deposited on the tricrystal (100) SrTiO₃ substrate, but before it was photolithographically patterned into rings, several microbridges (25 μm by 10 μm) across each bicrystal grain boundary, away from the tricrystal meeting point, were made to ascertain the overall junction quality. The approximate linear temperature dependence of normal-state resistance and the relatively high T_c values (~ 80 K) suggested that the film was near optimum doping (Fig. 2). The small shoulder below the sharp resistance drop is characteristic of a grain boundary weak link. The current-voltage (*I-V*) curve of this junction, measured at 4.2 K, exhibits a typical resistively shunted Josephson (RSJ) junction characteristic. The results of *I-V* measurements repeated on junctions located at various spots along the grain boundaries indicate that the grain boundary junctions mostly show RSJ behavior and the value of I_c is highly dependent on position, ranging from 1 μA to 0.5 mA.

To test the pairing symmetry, we patterned four rings (48 μm in inner diameter, 10 μm in width) using a standard photolithographic process (Fig. 1). To measure directly the magnetic flux threading through the rings, we used a high-resolution SSM (14). The microscope is composed of an integrated, miniature SQUID magnetometer and a mechanical scanning mechanism. In the microscope, a pickup loop (4 μm in loop diameter and 0.8 μm in line width) integrated into a low T_c SQUID sensor is mechanically scanned relative to the sample and the SQUID chip is inclined about 10° with respect to the sample plane. The sensor is mounted on a cantilever and scanned in direct mechanical contact with the sample. The distance between the contact point and the pickup loop center is

about 5 μm . The pickup loop structure is thus about 1 μm above the sample surface.

An SSM image of the four rings in the geometry of Fig. 1 was obtained at 4.2 K and in a nominal zero magnetic field (Fig. 3). There are several depressions in the SQUID signal, except for the zero-junction ring at the positions where the rings are interrupted by the grain boundaries. This indicates that these grain boundary junctions are weakly coupled and that the junction quality and uniformity varies from junction to junction. However, the fact that all the rings exhibit flux quantization for magnetic fields below 50 mG suggests that all the rings in this sample are indeed superconducting at low fields.

Determination of the quantum states.

To quantitatively analyze the magnetic flux quantum states of these rings, we used magnetic field titration (3). In response to a change of the externally applied magnetic field, a screening current is generated in a superconducting ring. By running the SSM line scans through the centers of the rings while varying the external field, one can plot the differences in sensor flux inside versus outside the ring, $\Delta\Phi_{\text{SQ}}$, for all the rings as a function of the applied field (Fig. 4A). From such magnetic field titration data, one can determine the gauge-invariant phase shift, ϕ_j , as well as the flux trapped in the ring. One can see that this is true by considering the free energy, U , of a superconducting π -ring (with a self-inductance L and a circulating current I) as a function of the flux threading the ring and the externally applied magnetic flux Φ_a :

$$U\left(\frac{\Phi}{\Phi_0}, \frac{\Phi_a}{\Phi_0}\right) = \frac{\Phi_0^2}{2L} \left\{ \left(\frac{\Phi}{\Phi_0}\right)^2 - \left(\frac{L|I_c|}{\pi\Phi_0}\right) \cos\left[\frac{2\pi}{\Phi_0}(\Phi + \Phi_a) + \pi\right] \right\} \quad (5)$$

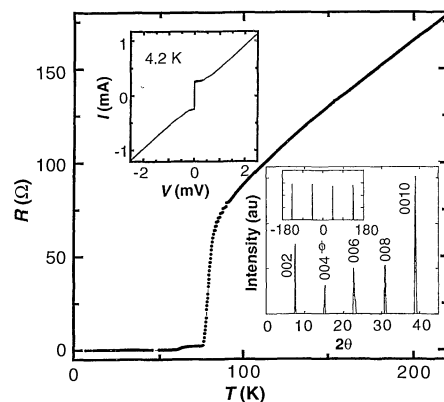


Fig. 2. The temperature dependence of electrical resistance, $R(T)$, for one of the grain boundary junctions in the Tl2201 *d*-wave tricrystal experiment. The *I-V* curve of this junction at 4.2 K is shown in the upper left inset. The XRD and ϕ -scan data are presented in the lower right inset; au, arbitrary units.

where $\Phi = LI$. Minimizing U against Φ gives the ground state of the ring. As shown by Sigrist and Rice (12) and others (11), the minimization of $U(\Phi, \Phi_a)$ with $\Phi_a = 0$, and for a π ring leads to a doubly degenerate ground state corresponding to $\pm\Phi_0/2$ spontaneous magnetization, provided that the LI_c product is much larger than Φ_0 (from here on we define $I_c = |I_c|$). The requirement of $LI_c \gg \Phi_0$ ensures that the cost of magnetic energy in maintaining $\pm\Phi_0/2$ spontaneous magnetization is well compensated for by the gain in Josephson energy (Eq. 5).

In other words, the phase difference induced across the junction to support the spontaneous magnetization current is insignificant compared to the gauge-invariant phase shift $\phi_j = \pi$, if $LI_c \gg \Phi_0$. For the case of a finite applied field, one can minimize the free energy $U(\Phi, \Phi_a)$ to obtain

values of ground-state flux Φ_m as a function of Φ_a . The sensor signal $\Delta\Phi_{SQ}$ is then related to Φ_m through

$$\Delta\Phi_{SQ} = M(0)\frac{\Phi_m}{L} \quad (6)$$

where $M(0)$ is the mutual inductance between the SQUID pickup loop (positioned above the center of the ring) and the ring. The results of such numerical calculations (Fig. 4B) show that Φ_m as a function of Φ_a invariably intercepts the horizontal axis ($\Phi_m = 0$) at $\Phi_a = 0.5\Phi_0$ for the case of $\phi_j = \pi$: a manifestation of a π -ring. The slope $d\Phi_m/d\Phi_a$ for $\Phi_a = 0.5\Phi_0$ at the intercept, however, varies greatly if $LI_c \lesssim \Phi_0$. In this case, the amount of flux trapped in the ring as measured by the vertical intercept is reduced significantly from its asymptotic value of $0.5\Phi_0$ for $LI_c \gg \Phi_0$. This finding indicates that fractional vortices arising from low- I_c π -junctions are possible and do not necessarily imply a violation in time-reversal symmetry (16).

With the aid of the results shown in Fig. 4B, one can now understand why, as shown in Fig. 4A, the titration curves for the three-junction ring intercept at exactly \pm half of the magnetic field spacing between the $\Delta\Phi_{SQ}(\Phi_a)$ curves for the zero-junction ring (in one quantum state) and the two-junction ring (in zero quantum state). On the other hand, the significantly reduced (by about 40%) slope of the $\Delta\Phi_{SQ}$ versus Φ_a curves at the intercept point suggests $LI_c \sim 0.3\Phi_0$ (Fig. 4B). This is consistent with our results of I_c measurements, which show that the values of I_c of the grain boundary junctions located along the 60° slant grain boundary are particularly low. The cause of low I_c may be oxygen deficiency, photolithography-induced degradation at the grain boundaries, or both. It is clear that the actual flux spontaneously generated at the tricrystal point of our ring samples can be substantially less than $\Phi_0/2$ if $LI_c \lesssim \Phi_0$.

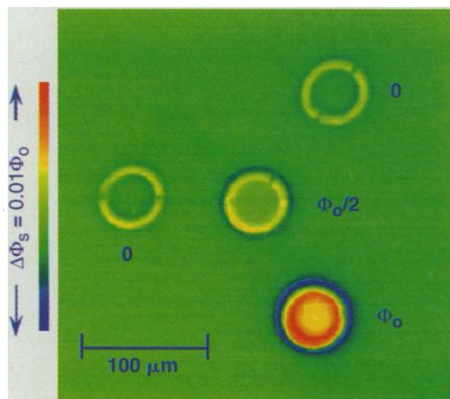


Fig. 3. SSM image of the four TI2201 rings (at 4.2 K and nominal zero magnetic field) in the geometry of Fig. 1. The flux quantum states of these rings are indicated in the figure.

However, as a convenience we will continue to use the generic term half-flux quantum effect to describe this effect in superconducting rings with π -phase shifts.

The spontaneous generation of half-flux quanta in the TI2201 tricrystal ring was further confirmed by repeating the experiment with a blanket film of TI2201 deposited on a (100) SrTiO₃ substrate of the same geometry as shown in Fig. 1. An SSM image of the sample cooled to 4.2 K in nominal zero magnetic field is shown in Fig. 5A. The full-scale range of the false colors corresponds to $0.025\Phi_0$ variation in the flux threading through the sensor SQUID pickup loop. This image is of a square of $200\ \mu\text{m}$ by $200\ \mu\text{m}$ with the tricrystal point at the center. An expanded view of the Josephson vortex trapped at the tricrystal point (Fig. 5B) shows that the vortex spreads along all three grain boundaries emanating from the tricrystal point. The spatial extent of the spread is a measure of the Josephson penetration length, λ_j . The unequal flux penetration along the grain boundaries suggests that the critical current density ($\propto \lambda_j^{-1/2}$) varies greatly from boundary to boundary.

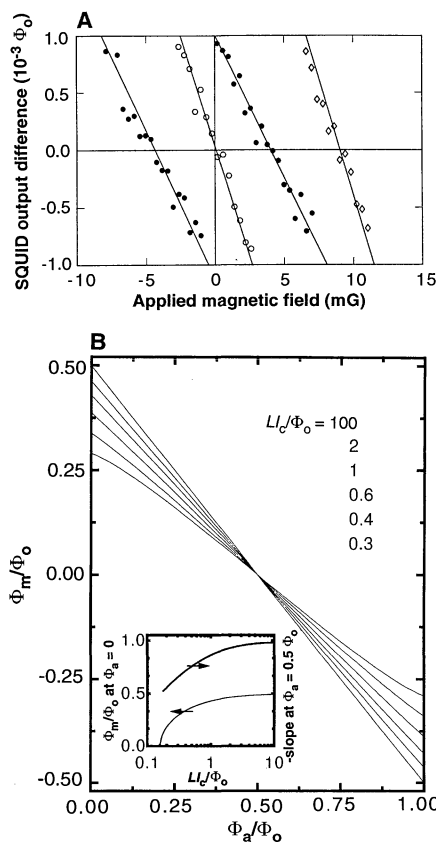


Fig. 4. (A) Differences in sensor flux inside versus outside the ring, $\Delta\Phi_{SQ}$, as a function of applied magnetic field for zero-junction (\times), two-junction (\circ), and three-junction (\bullet) rings. (B) Calculated ground-state flux Φ_m as a function of applied flux Φ_a in units of Φ_0 .

The spontaneous magnetization of half-integer flux quantum is a manifestation of the ground state of a π -junction superconducting system. Its occurrence should be independent of the macroscopic geometry of the tricrystal sample.

This point has been demonstrated recently by Kirtley *et al.* (17) with blanket YBCO films epitaxially grown on a tricrystal SrTiO₃ substrate by direct imaging integer flux ($h/2e$) Josephson vortices trapped in bicrystal grain boundaries and half-integer flux ($h/4e$) Josephson vortices only at the tricrystal intersection. The fact that only one half-integer Josephson vortex is trapped at the tricrystal point of the TI2201 blanket film suggests spontaneity and leads to the conclusion that the half-integer flux quantum effect is also observed in the tricrystal blanket film of TI2201. We have modeled the data present-

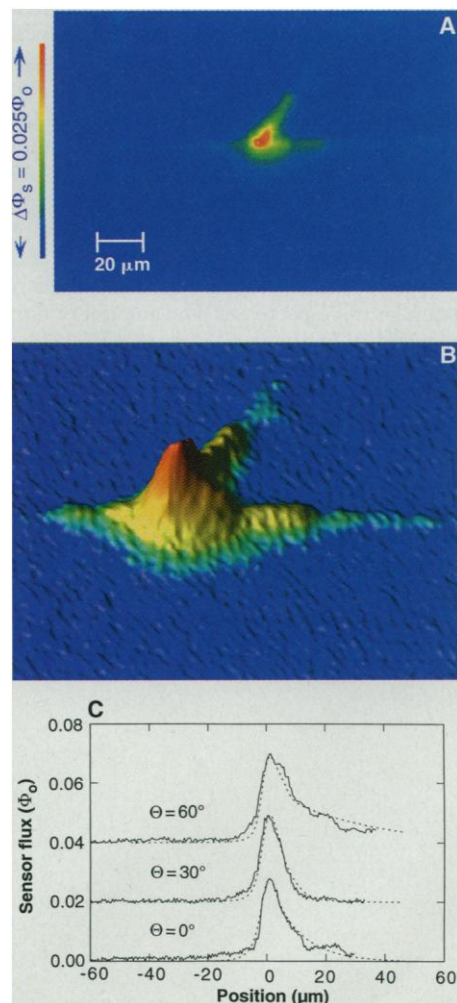


Fig. 5. (A) SSM image of a TI2201 blanket film deposited on a tricrystal (100) SrTiO₃ substrate of the same geometry as shown in Fig. 1 at 4.2 K and nominal zero magnetic field. (B) An expanded three-dimensional view of the Josephson vortex trapped at the tricrystal point. (C) The solid lines are the cross section (at an angle Θ with respect to the horizontal grain boundary) through the data in Fig. 5A. The dashed lines are fits of Eq. 5 to the data.

ed in Fig. 5A following the procedure used for YBCO (17) to determine the total amount of flux at the tricrystal point. The magnetic fields at the surface of the sample, a distance r_i from the tricrystal point along the i th grain boundary, are given by

$$B_z(r_i, r_\perp) = \frac{2\Phi_0 a_i}{\pi \lambda_L (\lambda_J)_i} \frac{e^{-r_i/(\lambda_J)_i}}{(1 + a_i^2 e^{-2r_i/(\lambda_J)_i})} e^{-r_\perp/\lambda_L} \quad (7)$$

where r_\perp is the perpendicular distance from the grain boundary, $(\lambda_J)_i$ is the Josephson penetration depth along the i th grain boundary, λ_L is the bulk London penetration depth, and a_i is a normalization constant chosen such that $a_i/[(\lambda_J)_i(1 + a_i^2)]$ is the same for all three grain boundaries, and the total flux at the tricrystal point is $\Phi_{\text{tot}} = \sum_i (\Phi_0/2\pi) 4\pi \tan^{-1}(a_i)$. The flux through the pickup loop is calculated by numerical integration over the known geometry of the loop as calibrated by imaging bulk superconducting vortices. In Fig. 5C, the solid lines are the cross sections (at an angle Θ with respect to the horizontal grain boundary) through the data in Fig. 5A. The dashed lines are fits of Eq. 7 to the data, with fitting parameters of the total flux of the Josephson vortex $0.42\Phi_0$, $\lambda_J = 6, 10,$ and $26 \mu\text{m}$ for the left, right, and diagonal grain boundaries, respectively. The amount of flux required to fit the data is about 17% below $\Phi_0/2$. It is worth noting, however, that this is nearly the same reduction that we found for YBCO and may simply represent a systematic error due to, for example, the finite thickness effect in our analysis. The fact that this value is closer to $\Phi_0/2$ than that observed for the rings may be due to the fact that no lithography was required to prepare the blanket film sample, providing less opportunity for the grain boundaries to degrade.

We have run eight Tl2201 samples. The

materials problems associated with this system are formidable, and the results from six of the samples were discarded because sections of the films were not superconducting, there was substantial inhomogeneous flux trapping in the grain boundaries, or the rings did not support superconducting screening currents. In two of the samples, the results of which we have presented here, these problems were not evident. The SSM's ability to directly image local magnetic field distribution allowed us to unambiguously discriminate between high- and low-quality samples without being confused by spurious flux trapping. This is a true advantage of scanning SQUID microscopy over other methods that detect only the average flux.

As pointed out in our earlier work on the YBCO system (2, 11), the present design of the tricrystal substrate cannot rule out even-parity states with an order parameter varying as $\cos 4\theta$ (the so-called g -wave pairing). A separate g -wave-only tricrystal experiment (11) has been done for the YBCO system, and the absence of the half-integer flux quantum effect in that experiment has ruled out the g -wave pairing. In view of this result and based on a universality argument, g -wave pairing in Tl2201 is not very likely. This is indeed the case, as confirmed by an experiment with a blanket coverage of a Tl2201 film on a g -wave-only tricrystal substrate. Our SSM images never showed any flux trapped at the tricrystal point, as would be expected for a superconductor with g -wave pairing symmetry.

In the future, a systematic study as a function of doping with the d -wave tricrystal geometry should be carried out in the Tl2201 system to study the band structure effect on pairing symmetry. Also, it is of great interest to study possible macroscopic quantum tunneling between the bistable $\pm\Phi_0/2$ states in a π -ring with very low LI_c .

REFERENCES AND NOTES

1. D. A. Wollman, D. J. van Harlingen, W. C. Lee, D. M. Ginsberg, A. J. Leggett, *Phys. Rev. Lett.* **71**, 2134 (1993).
2. C. C. Tsuei *et al.*, *ibid.* **72**, 593 (1994).
3. J. R. Kirtley *et al.*, *Nature* **373**, 225 (1995).
4. A. Mathai, Y. Gim, R. C. Black, A. Amar, F. C. Wellstood, *Phys. Rev. Lett.* **74**, 4523 (1995).
5. D. A. Brawner and H. R. Ott, *Phys. Rev. B* **50**, 6530 (1994).
6. J. H. Miller Jr. *et al.*, *Phys. Rev. Lett.* **74**, 2347 (1995).
7. D. A. Wollman, D. J. van Harlingen, J. Giapintzakis, D. A. Ginsberg, *ibid.*, p. 797.
8. D. Z. Liu, K. Levine, J. Malay, *J. Supercond.* **8**, 663 (1995). *Phys. Rev. B* **51**, 8680 (1995).
9. A. I. Liechtenstein, I. I. Mazin, O. K. Andersen, *Phys. Rev. Lett.* **74**, 2303 (1995); A. A. Golubov and I. I. Mazin, *Physica C* **243**, 153 (1995).
10. R. Combescot and X. Leyronas, *Phys. Rev. Lett.* **75**, 3732 (1995); K. Kuboi and P. A. Lee, *J. Phys. Soc. Jpn.* **64**, 3179 (1995).
11. C. C. Tsuei *et al.*, in *Proceedings of the Stanford Conference on Spectroscopies in Novel Superconductors* (15 to 18 March 1995).
12. M. Sigrist and T. M. Rice, *J. Phys. Soc. Japan* **61**, 4283 (1992).
13. V. B. Geshkenbein, A. I. Larkin, A. Barone, *Phys. Rev. B* **36**, 235 (1987).
14. J. R. Kirtley *et al.*, *Appl. Phys. Lett.* **66**, 1138 (1995).
15. C. A. Wang, Z. F. Ren, J. H. Wang, W. Y. Yu, A. Petrou, unpublished results.
16. Any spontaneous flux generated due to broken time reversal symmetry is present even in the limit as the loop inductance goes to zero, unlike in the case of simple d -wave symmetry. M. R. Beasley, D. Lew, R. B. Laughlin, *Phys. Rev. B* **49**, 12330 (1994); M. Sigrist, D. B. Bailey, R. B. Laughlin, in preparation.
17. J. R. Kirtley *et al.*, *Phys. Rev. Lett.*, in press.
18. The authors wish to thank L.-S. Yu-Jahnes, C. C. Chi, D. M. Newns, K. A. Moler, R. Koch, J. R. Clem, and C. M. Varma for useful discussions, and C. A. Pickover for computer image processing of Fig. 5B. The technical assistance of S. L. Brown and G. Trafas is greatly appreciated. The scanning SQUID microscope used for this work was partially supported by the Consortium for Superconducting Electronics, with funding from the Advanced Research Projects Agency Contract No. MDA972-90-C-0021. The work at SUNY Buffalo was supported in part by the New York State Institute on Superconductivity and the New York State Energy Research and Development Authority. M.B. acknowledges support from the University Research Initiative of the Department of Defense through the U.S. Air Force Office of Scientific Research.

16 October 1995; accepted 7 December 1995